

Geoacoustic Inversion of Tow-Ship Noise via Near-Field–Matched-Field Processing

David J. Battle, *Member, IEEE*, Peter Gerstoft, *Member, IEEE*, William A. Kuperman, William S. Hodgkiss, *Member, IEEE*, and Martin Siderius

Abstract—This paper discusses geoacoustic inversion from tow-ship noise data acquired via a horizontal towed array. Through simulations and experimental results, it is shown that even very quiet ships radiate sufficient noise power to enable self-noise inversion of basic geoacoustic parameters such as effective bottom velocity. The experimental results presented are particularly encouraging in view of the high level of interference shown to be tolerated from nearby shipping.

Index Terms—Geoacoustic inversion, self-noise, tow ship.

I. INTRODUCTION

THE estimation of geoacoustic parameters of marine sediments and subsediment layers involves the measurement of acoustic fields in the ocean waveguide for comparison with accurate forward propagation models. Conventionally, the data upon which inversions are based are acquired from vertical arrays in the far field of the source, yielding parameter estimates averaged over the intervening environment. While vertical array technology and associated techniques have reached a high level of refinement, horizontal arrays towed by ships present definite operational advantages in terms of mobility and localization of measurement [1]–[4]. Spot measurements of geoacoustic parameters, sensitive only to bottom conditions between a tow ship and array, can form useful inputs to range-dependent propagation models and geophysical surveys.

Commonly, scientific and commercial applications of towed arrays have required dedicated acoustic sources to be towed in addition to the array. Such dedicated sources, along with their high-power control equipment, add expense and complexity to geoacoustic surveying. This has led to interest in *self-noise* inversion, wherein plant and hydrodynamic noise generated by the tow ship itself is received on the array and processed to extract estimates of local geoacoustic parameters such as bottom velocity [5], [6]. An introduction to the self-noise inversion problem and associated physics can be found in [1].

Manuscript received July 10, 2002; revised November 27, 2002. This study was supported by NAVSEA/ASTO under ONR contract N00014-01-D-0043.

D. J. Battle was with The Marine Physical Laboratory, University of California—San Diego, La Jolla, CA 92093-0238 USA. He is now with the Massachusetts Institute of Technology, Cambridge, MA 02139, USA (e-mail: david.battle@ieee.org).

P. Gerstoft, W. A. Kuperman, and W. S. Hodgkiss are with The Marine Physical Laboratory, University of California—San Diego, La Jolla, CA 92093-0238 USA (e-mail: davidb@mpl.ucsd.edu).

M. Siderius was with the SACLANT Undersea Research Centre, La Spezia, Italy. He is now with the Ocean Sciences Division, Science Applications International Corporation, La Jolla, CA 92037 USA.

Digital Object Identifier 10.1109/JOE.2003.816679

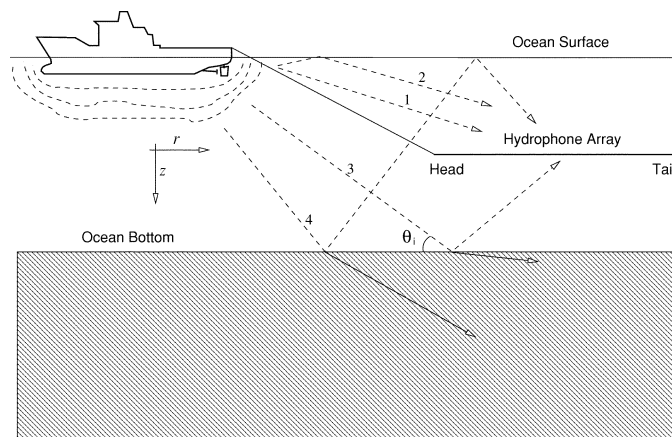


Fig. 1. Typical geometry for shallow water towed-array operations showing the dominant four arrivals of rays from the tow ship at the array. The angle θ_i is the grazing angle of incidence at the bottom.

This paper sets out to examine self-noise geoacoustic inversion from the standpoint of near-field–matched-field processing (MFP) and, in particular, the sensitivity of the reconstructed source power to perturbations in the parameters of a short-range propagation model. Solution of the geoacoustic inversion problem itself is then posed in a multiparameter optimization framework and solved via an efficient global search based on genetic algorithms (GA).

To investigate the robustness of the proposed inversion method, effective bottom velocities are estimated from experimental data acquired during an experiment conducted north of the island of Elba in 2000. The results obtained are encouraging, not least because they represent the worst case scenario involving a very quiet tow ship operating at low speed amid severe interference from nearby shipping.

II. GEOACOUSTIC INVERSION USING TOWED ARRAYS

Since their inception during World War I, towed arrays have always been separated from their tow platforms by substantial distances to minimize self-noise interference. In geoacoustic applications as well, large range separations are required, which will be shown to be a geometric requirement of environmental sensitivity. Fig. 1 illustrates the typical configuration of a towed acoustic array in shallow water. The array itself would commonly measure hundreds of meters in length and consist of tens to hundreds of hydrophones organized in groups of low- and high-frequency sensitivity. Such arrays are usually neutrally buoyant so as to achieve a stable horizontal configuration [7].

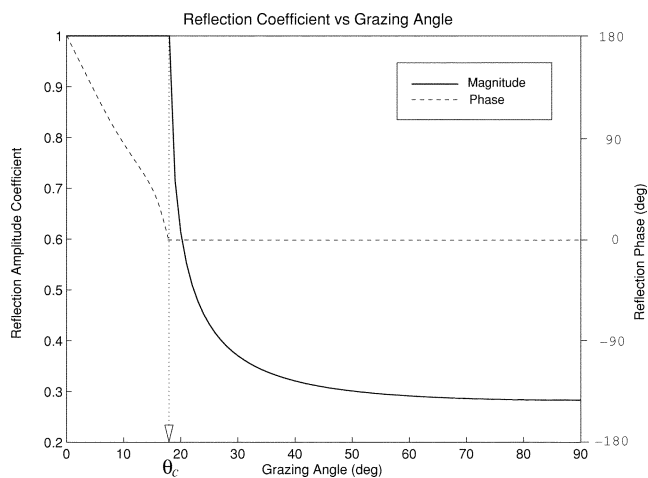


Fig. 2. Theoretical variation in bottom-reflection coefficient in amplitude and phase with respect to grazing angle. The bottom parameters considered were $c_b = 1600$ m/s, $\rho_b = 1700$ kg/m³, and $\alpha_b = 0$ dB/ λ .

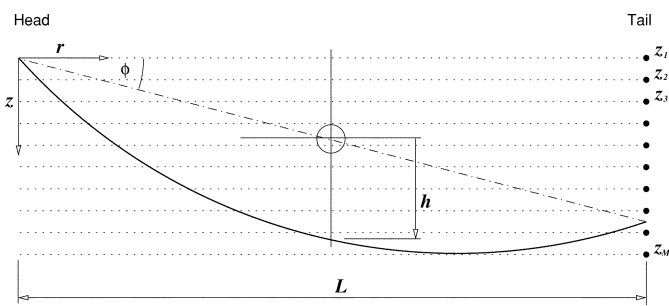


Fig. 3. Parabolic array model including parameters of tilt ϕ and bow h . Transfer functions to each of the $N = 128$ array elements are linearly interpolated from transfer function evaluations at M depths.

Instrumented pressure sensors inside the array are used to monitor array depth, while some more-sophisticated arrays intended specifically for seismic exploration have hydrodynamic vanes or *birds* to provide positive depth control.

Also shown in Fig. 1 are the ray paths of the dominant acoustic arrivals of ship-generated noise at the array. Any information pertaining to the geoacoustic properties of the bottom must be associated with the bottom-interacting paths, numbered here as three and four. At issue, therefore, is the nature of the interaction between the tow-ship field and the ocean bottom, which, to first order, will be characterized by a simple acoustic half space. In depicting the propagation paths in Fig. 1 as straight lines, a further implicit assumption is that the water column is effectively iso-velocity over the scales of range and depth considered. This leads to the well-known Pekeris waveguide environment, which, while assisting in clarity of presentation, does not limit the application of the proposed inversion method. In principle, any complexity of layering in the parameters of compressional velocity c_p , density ρ , and attenuation α can be incorporated into the forward propagation model and extensions to visco-elastic layering are straightforward.

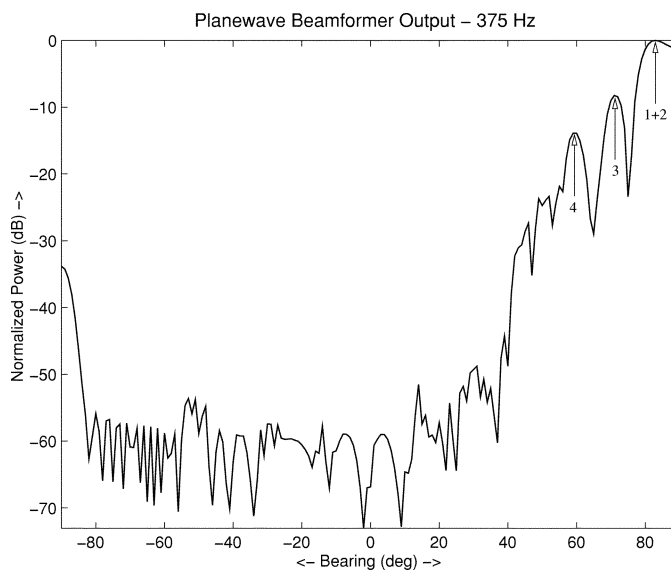


Fig. 4. Conventional plane-wave beamformer response to simulated towed-array data. The numbered lobes correspond to the ray paths of Fig. 1. Positive bearings are in the direction of the tow ship.

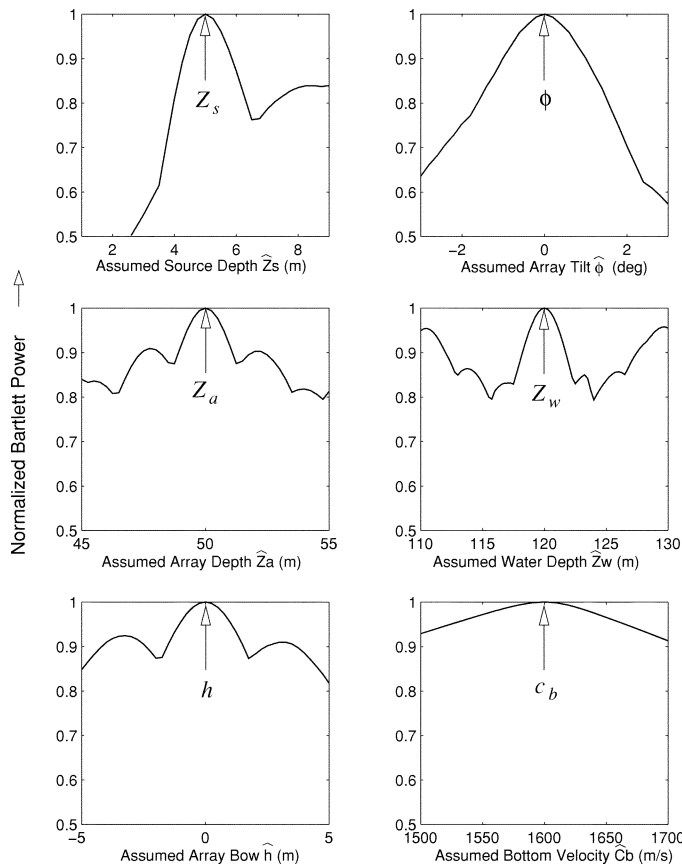


Fig. 5. Modeled Bartlett power variations for perturbations to Pekeris environment parameters. $z_w = 120$ m, $z_s = 5$ m, $z_a = 50$ m, $c_b = 1600$ m/s, and $\rho_b = 1700$ kg/m³. Source-array range = 400 m.

Having simplified the acoustic environment to this extent, it is apparent that the nature of the interaction between the tow-ship field and the bottom is completely described by the reflection

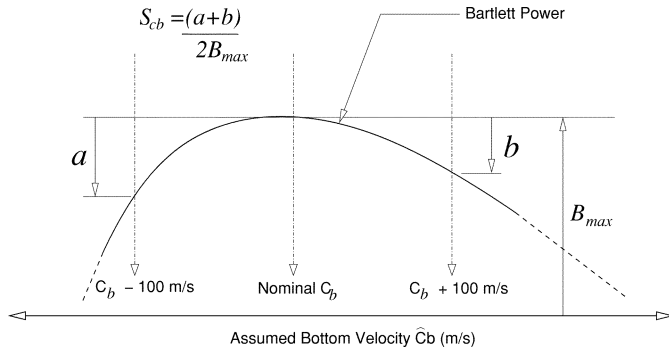


Fig. 6. Definition of normalized Bartlett power sensitivity S_{cb} .

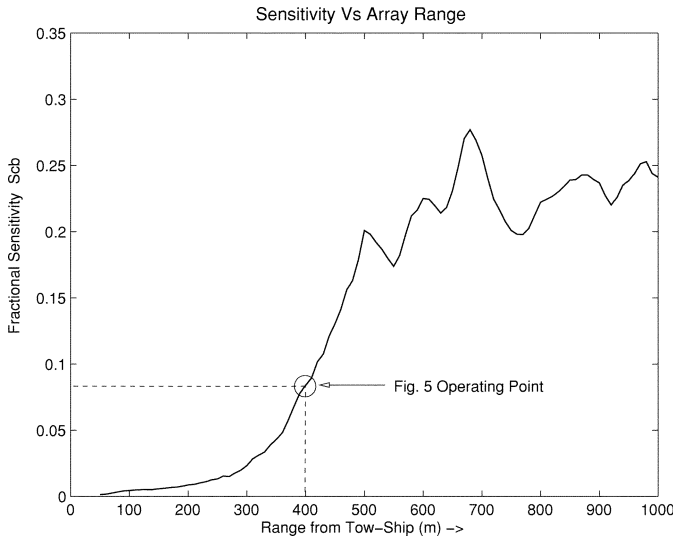


Fig. 7. Modeled Bartlett power sensitivity S_{cb} versus source-array range. Environmental parameters were the same as those used in Fig. 5.

coefficient of the water-bottom interface. This can be expressed by [8]

$$R = \frac{\rho_b k_{z,w} - \rho_w k_{z,b}}{\rho_b k_{z,w} + \rho_w k_{z,b}} \quad (1)$$

where the vertical wavenumbers in the water and bottom, $k_{z,w}$ and $k_{z,b}$, respectively, are related to the grazing angles of incidence and transmission θ_i and θ_t by

$$k_{z,w} = k_w \sin \theta_i \text{ and } k_{z,b} = k_b \sin \theta_t \quad (2)$$

where $k_w = \omega/c_w$ and, allowing for a plane wave attenuation of α_b nepers/m in the bottom, $k_b = \omega/c_b + i\alpha_b$. For the particular case of a hard bottom (i.e., $c_w < c_b$) the so-called *critical angle* of incidence, defined by

$$\theta_c = \arccos \left(\frac{c_w}{c_b} \right) \quad (3)$$

separates the reflectivity function into two distinct regions, as illustrated by Fig. 2, which assumes zero-bottom attenuation and other Pekeris parameters roughly comparable with those encountered in the experiment to be discussed later in Section VII.

With reference to Figs. 1 and 2, it can be seen that, up to the critical angle θ_c (meaning beyond a certain critical range from the tow ship), propagation is best described in waveguide terms, where bottom interacting waves are well reflected with little

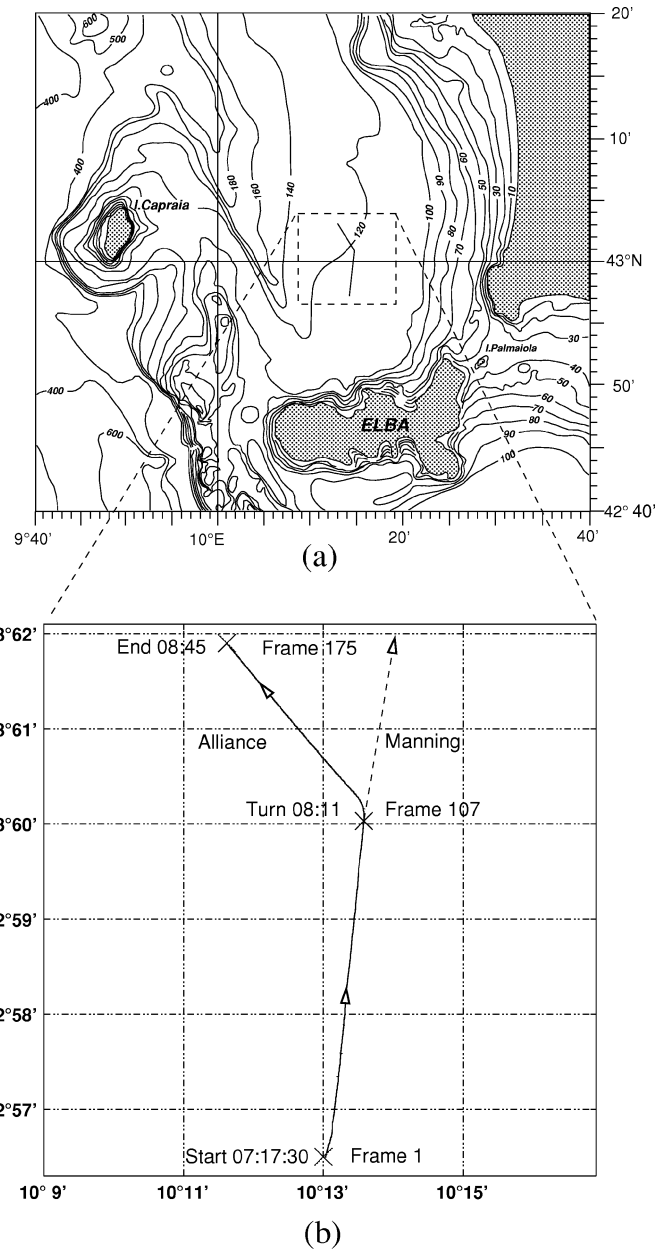


Fig. 8. The tracks of the NRV ALLIANCE and MANNING during the experiment. All times are UTC. Each frame represents 30 s.

energy penetrating into the bottom. The range dependence of the tow-ship field received by the array is, therefore, mostly a function of bottom-reflection phase, which is seen to have an almost linear dependence on θ_i with a gradient set by θ_c (and, hence, c_b). At closer ranges, where the bottom arrivals are steeper than θ_c , the distribution of energy received by the array is again a function of θ_i , but the variation is mainly in terms of reflection amplitude. A particular pattern of amplitudes received along the array can, in principle, be associated with a unique value of bottom half-space velocity. Conversely, while affecting the near field in absolute terms through the impedance contrast, the bottom density does not significantly affect the array field *pattern*. Similarly, in the near field, the influence of bottom attenuation is very small.

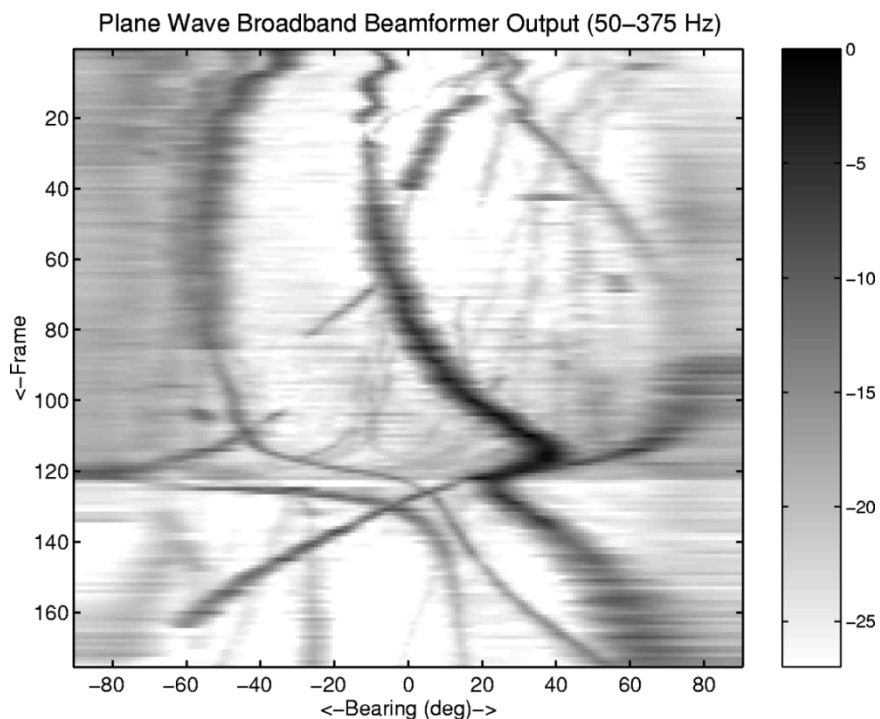


Fig. 9. Broad-band beamformer power (decibels) versus frame along the track shown in Fig. 8. All bearings are relative to the array. Bearings in the ALLIANCE direction are positive.

III. PROPAGATION MODELING

Accurately modeling the response of acoustic environments is a principal aspect of geoacoustic inversion. In the present case of towed-array inversion, particular attention is required to aspects of short-range propagation that differentiate it from long-range waveguide propagation; namely, the leaky *virtual modes* that result from super-critical angles of bottom incidence [1]. In view of this and the somewhat relaxed concern regarding range dependence over short distances, the classical full-wave approach of wave-number integration was selected here to model the propagation of tow-ship noise to the towed array.

A. Wavenumber Integration

The following is a brief review of the theory behind the wavenumber integration or *spectral* approach to modeling acoustic propagation in horizontally stratified media. For detailed descriptions, the reader is directed to [8] and [9]. With the assumption of purely horizontal stratification and point sources and receivers, the inhomogeneous form of the wave equation can be depth-separated in cylindrical coordinates to yield [8]

$$\left[\frac{d^2}{dz^2} + (k_m^2 - k_r^2) \right] \psi(k_r, z) = S_\omega \frac{\delta(z - z_s)}{2\pi} \quad (4)$$

where k_r is a horizontal wavenumber related to the medium wavenumbers k_m and vertical wavenumbers k_z via

$$k_z = \sqrt{k_m^2 - k_r^2} \quad (5)$$

and S_ω is the strength of a source at depth z_s at radian frequency ω . Assuming a coupled stack of locally homogeneous layers, the solution to (4) can be expressed in each layer as a sum of up-

ward- and downward-propagating conical waves. These waves, of the form

$$H_\omega(k_r, z) = A^+(k_r) \exp(jk_z z) + A^-(k_r) \exp(-jk_z z) \quad (6)$$

when added to corresponding components of the free-space Green's function in the source layer

$$g_\omega(k_r, z, z_s) = -\frac{\exp(jk_z |z - z_s|)}{4\pi jk_z} \quad (7)$$

must satisfy the boundary conditions of continuous vertical displacement w and normal stress σ_{zz} at all boundaries. In this study, the plane-wave amplitude coefficients A^- and A^+ were determined for successive layers via the propagator matrix approach due to Thomson [10] and Haskell [11], taking particular care to use analytic matrix inverses for improved numerical stability [8]. After determining the solution to (4) at successive values of k_r , the result is a depth-dependent Green's function in wave-number space. Computation of the exact array pressure field in range would then require an inverse Hankel transform of the form

$$g_\omega(r, z) = \int_0^\infty g(k_r, z) J_0(k_r r) k_r dk_r \quad (8)$$

where J_0 is a Bessel function of the first kind of order zero. Given the simple exponential asymptotic form of the outward propagating part of J_0 beyond a few wavelengths, the so-called Fast-Field approximation to the exact inverse Hankel transform was used here, as detailed in [8]. Evaluation of (8) over a discrete set of equally spaced ranges is then accurately approximated via a single fast Fourier transform (FFT) of the wavenumber kernel.

In view of the simplicity of the bottom structure assumed in this initial study, the use of wavenumber integration for forward-propagation modeling may appear to be more sophisti-

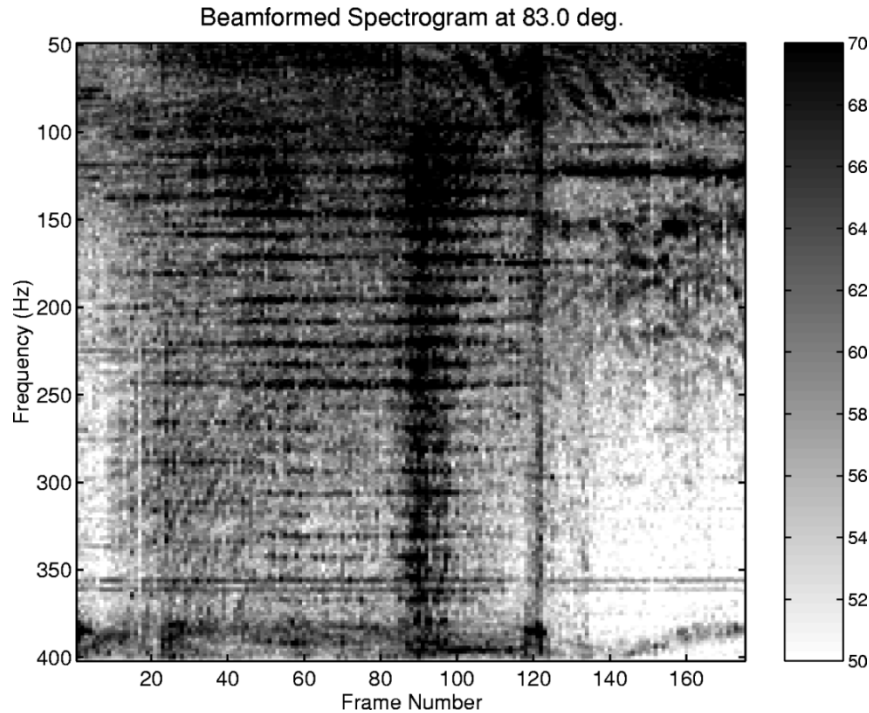


Fig. 10. Spectrograms (dB re 1 μ Pa) beamformed in the approximate direct-path direction of the tow ship ALLIANCE (83°).

cated than warranted; however, it is intended that future study will deal with more complex environments, which will require the full flexibility of such a treatment.

B. Array Model

Using the above approach, a single FFT of a wavenumber kernel yields complex pressures (or transfer functions) at evenly spaced ranges from a point source at a single depth. Anticipating the requirements of analyzing the experimental data in Section VII, a numerical model incorporating the possibility of multiple independent sources and 128 hydrophone receivers at 2-m spacings was used.

Although it was stated in Section II that towed arrays are usually operated with a fair degree of control, it was viewed as important from the standpoint of real-data analysis to allow for likely geometric distortion of the array from its ideal horizontal and straight configuration. So as not to overly complicate the array model, however, only the two additional parameters of tilt and bow were added.

Fig. 3 is an illustration of the towed-array model as implemented here, with the value of array depth z_a relating to the head (towed end). The straight line connecting the array endpoints is assumed to be tilted through ϕ degrees, with the parabolic array shape parameterized by the bow h of the array below its midpoint. In terms of the local coordinate system of the array, r is taken to be the horizontal range of each element from the array head. The approximate array shape, assuming that the horizontal length L does not change appreciably under the very small distortions intended to be modeled, is given by

$$z_r = \frac{4h}{L^2} (L - r)r + r \sin \phi. \quad (9)$$

Transfer function evaluations from the ship source(s) to each of the array elements were linearly interpolated in amplitude and phase from a small number of solutions to (8) at depths z_m ($m = 1, \dots, M$) spaced at depth intervals not exceeding $\lambda/4$. For simulation purposes, the numerical model described is capable of synthesizing broad-band time series of arbitrary length for each array hydrophone from an arbitrary number of point sources.

For the purpose of unifying the intuitive picture of short-range propagation between the tow ship and array given by Fig. 1 with the wave theory solution, the numerical model described above was run with the following parameters: water depth $z_w = 120$ m, source depth $z_s = 5$ m, array depth $z_a = 50$ m, bottom velocity $c_b = 1600$ m/s, bottom density $\rho_b = 1700$ kg/m³, and compressional wave attenuation $\alpha_b = 0$ dB/ λ . The array was assumed to be horizontal and straight. For wavenumber integration, an FFT size of 2048 points was used and the range increment dr was set to the array element spacing of 2 m ($L = 254$ m). A single time-harmonic source at 375 Hz was modeled at a range of 400 m. Fig. 4 illustrates the result of applying conventional plane-wave beamforming to the simulated array data. Along with the single broad lobe associated with the direct and surface reflected arrivals near endfire, additional lobes are resolved, corresponding to paths 3 and 4 in Fig. 1. By virtue of the reflection coefficient behavior, arrival strength is seen to be progressively attenuated at steeper angles, with no clear multipath structure evident within 40° of vertical (array broadside).

IV. MATCHED FIELD PROCESSING

The approach to matched field processing taken here is conventional and uses the standard Bartlett processor to calculate

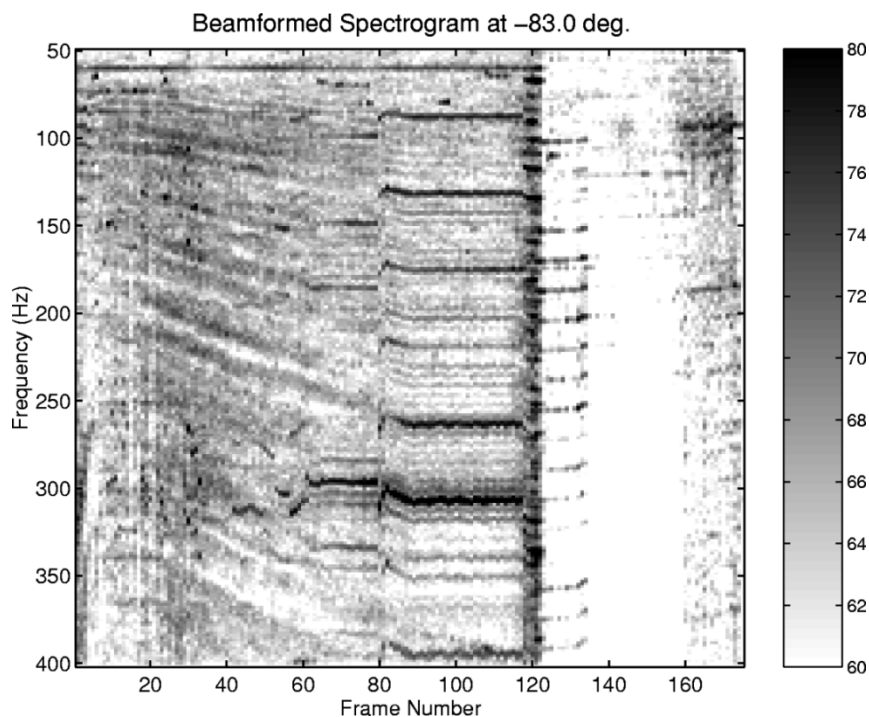


Fig. 11. Spectrograms (dB re $1 \mu\text{Pa}$) beamformed in the approximate direct-path direction of the chase-ship MANNING (-83°).

powers over a set of hypothesized source locations [8]. The inputs to the calculation are the estimated cross-spectral density matrices, denoted $\hat{\mathbf{R}}_i$ ($i = 1, \dots, K$), which are averaged from N snapshot (column) vectors $\mathbf{d}_{n,i}$ of the array data at frequencies ω_i according to

$$\hat{\mathbf{R}}_i = \frac{1}{N} \sum_{n=1}^N \mathbf{d}_{n,i} \mathbf{d}_{n,i}^\dagger \quad (10)$$

and corresponding sets of replica vectors $\mathbf{w}_i(\mathbf{m})$, calculated from the forward acoustic model and parameterized by the environmental vector \mathbf{m} . This vector included both geometric parameters, such as unknown or poorly known depths, as well as acoustic parameters such as velocities, densities, and attenuations. For each forward-model evaluated, the source range was optimized by finding the range corresponding to the maximum objective function in a prearranged search window. Thus, the source range was treated as a nuisance parameter and not explicitly included in the optimization.

The normalized multifrequency output of the Bartlett processor, given by

$$B(\mathbf{m}) = \frac{1}{K} \sum_{i=1}^K \left[\frac{\mathbf{w}_i^\dagger(\mathbf{m}) \hat{\mathbf{R}}_i \mathbf{w}_i(\mathbf{m})}{\text{tr}[\hat{\mathbf{R}}_i] \|\mathbf{w}_i(\mathbf{m})\|^2} \right] \quad (11)$$

is, in effect, the square of the correlation coefficient between the averaged data vectors and the replica vectors computed for each environment tested. Values approaching unity imply a near-perfect match between the measured and modeled environments and, hence, a high probabilistic likelihood of the environmental parameters being correct. Values near zero imply either that the parameters are far from correct, that the parameterization

is wrong, or that the level of interference in the measured data is high. In the optimizations carried out to select the most likely geoacoustic parameters, (11) is used as the objective function.

Caiti *et al.* [2] demonstrated the concept of MFP inversion with a towed array (156-m aperture) using narrow-band data. The feasibility test was successful, but several problems with the method were described in their concluding remarks. Among the most serious difficulties encountered were array shape deformation, low sensitivity to the bottom parameters, and balancing of the tradeoff between computational efficiency and accuracy of the inversion solution. With the additional flexibility provided by the array model used here, we aim to address some of these problems. In Section V, the issue of parameter sensitivity is viewed from a modeling perspective so that the issues affecting it can be clarified.

V. MODEL PARAMETER SENSITIVITY

Having defined the Bartlett objective function in Section IV, it is possible to evaluate the inherent sensitivity of a typical towed-array geometry to several parameters; namely, the water, array, and source depths, z_w , z_a , and z_s ; the array tilt and bow, ϕ and h ; and most importantly, the bottom velocity c_b . This has been accomplished in Fig. 5 by simulating array data for the same set of environment and array parameters used in Section III-B. Line searches around the nominal parameter values are seen to perturb the objective function to varying degrees for each parameter. For the modeled source-array range of 400 m, which is a realistic towing distance for a 254-m-long array, most of the eigenrays would have bottom-grazing angles $\theta_i > \theta_c = 18.2^\circ$, which corresponds to $c_b = 1600$ m/s. The same is true for a perturbed velocity of 1700 m/s, the highest assumed, which gives $\theta_c = 26.6^\circ$. With reference to Fig. 2, it is apparent that,

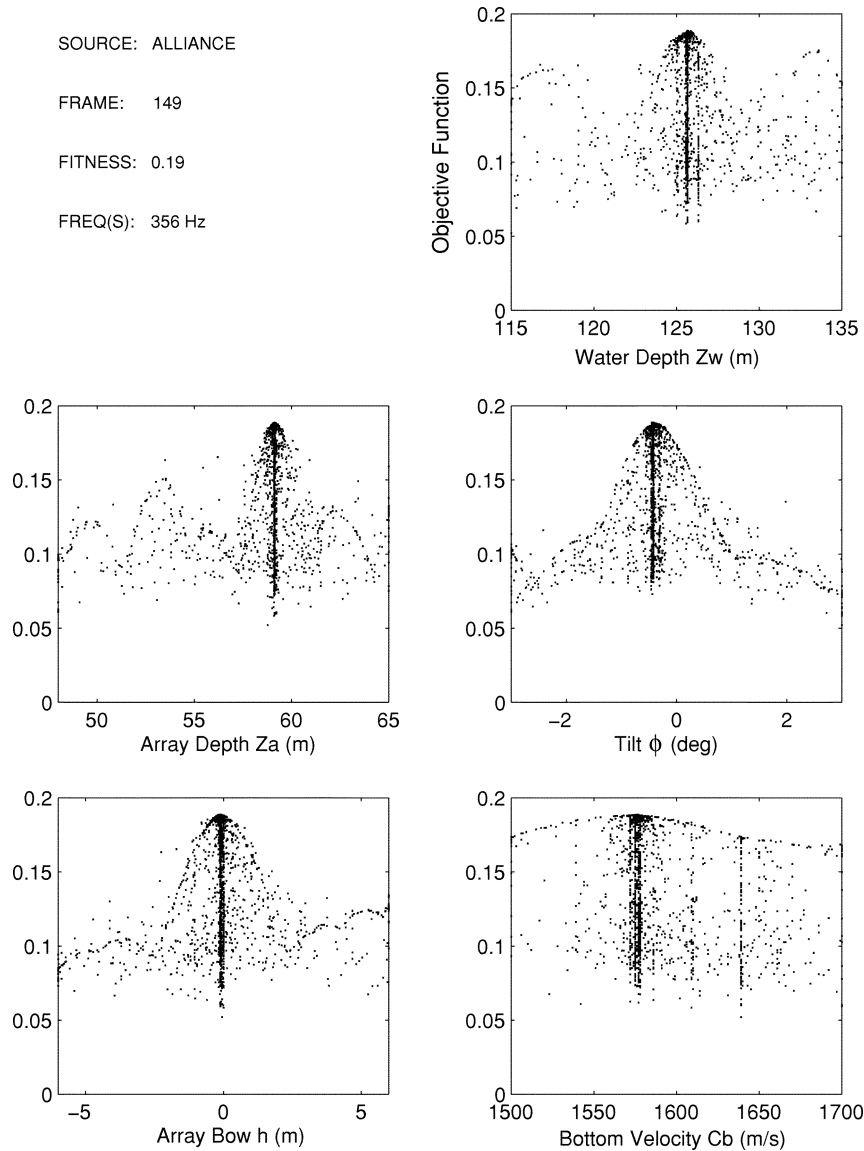


Fig. 12. Scatter plots of GA search for frame 149 (ALLIANCE source).

as the range of the array increases, and more eigenrays are incident at $\theta_i < \theta_c$, the variation in the amplitudes of reflected waves received over the length of the array increases. Furthermore, the reflection coefficient R , as a function of grazing angle θ_i , is most sensitive *in amplitude* to variations in θ_c (and, hence, c_b) in this region.

For the source-array range of 400 m modeled here, the Bartlett power can be seen to vary by less than 10% of its peak value for a ± 100 m/s variation in c_b . This exemplifies a suboptimal regime in that a greater array range would result in more sensitivity to c_b . In contrast, for this case, the Bartlett power is seen to be very sensitive to source depth and array tilt. Source depth, which is usually known with some degree of certainty for a surface ship, would be expected to be a sensitive parameter, as Bartlett power varies rapidly in the vicinity of a pressure-release boundary.

Although geometric parameters such as z_a and z_s have sensitivities of their own, which can be expected to vary with the environment, they are effectively nuisance parameters in that the

main objective here is to determine the bottom compressional wave velocity c_b . Concentrating on this parameter and defining the fractional sensitivity S_{cb} of the normalized Bartlett power to the bottom velocity, as shown in Fig. 6, S_{cb} is observed to increase rapidly as the source-array range approaches the critical range that results in more eigenrays incident at $\theta_i < \theta_c$. From Fig. 7, it is also apparent that beyond approximately 500 m, which corresponds to $\theta_i = 20.3^\circ$ in Fig. 2, S_{cb} saturates and then oscillates as the dependence of R on θ_i switches from amplitude to phase, marking the onset of full waveguide propagation and its associated constructive and destructive interference between discrete modes.

VI. PARAMETER OPTIMIZATION

As evident from Fig. 5, variations in the Bartlett power objective function can be multimodal, even for some single-parameter variations. Hence, optimization algorithms for the full multidimensional function must contend with local maxima, which

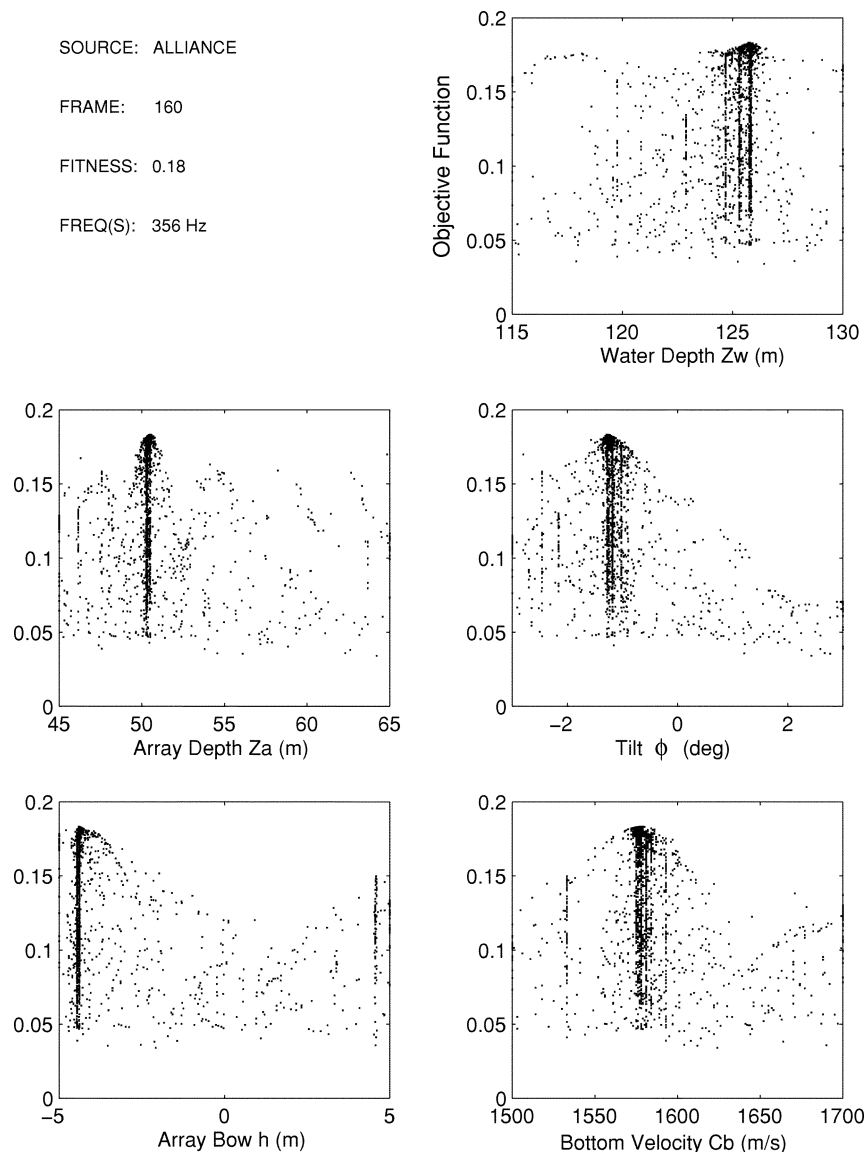


Fig. 13. Scatter plots of GA search for frame 160 (ALLIANCE source).

do not correspond to globally optimal parameters. The purpose of this section is not to make an in-depth presentation of the particular genetic optimization approach used here, as such algorithms are now standard tools of geoacoustic inversion [12], [13]. Rather, it is intended to record the authors' experience that, even for short-range geoacoustic inversion problems with small numbers of paths between the source and array, calculus-based local optimization approaches perform poorly.

In this study, purely local optimization algorithms were first investigated as means of selecting environmental parameters. Ultimately, however, the most-successful approach found was a guided Monte Carlo search using GAs. Not only did GA appear to converge reliably, but records of the objective function obtained versus the parameter values searched were found to offer valuable insights into the global properties of the objective function. From the density of samples in various projections of these plots, the reliability of individual inverted parameters can be judged. Although probabilistic considerations such as these are beyond the scope of this paper, the interested reader is di-

rected to [14] and [15]. For further information regarding geoacoustic applications of GA optimization in general, the reader is directed to [13].

VII. EXPERIMENTAL SELF-NOISE INVERSION

The 90-min experiment discussed here was conducted by the SACLANT Undersea Research Centre and the Marine Physical Laboratory as part of MAPEX2000, which was specifically directed at validating a range of array-processing and geoacoustic-inversion techniques. The data were acquired north of the island of Elba, off the Italian west coast on November 29, 2000 between the times of 07:17:30 and 08:45:00 UTC. The array used consisted of 128 hydrophones evenly spaced at 2 m. Half-wavelength sampling therefore occurred at approximately 375 Hz. Depth control with this array proved less accurate than hoped, although this turned out to be of little consequence, as both z_a and z_w were included in the vector \mathbf{m} along with the other parameters to be optimized.

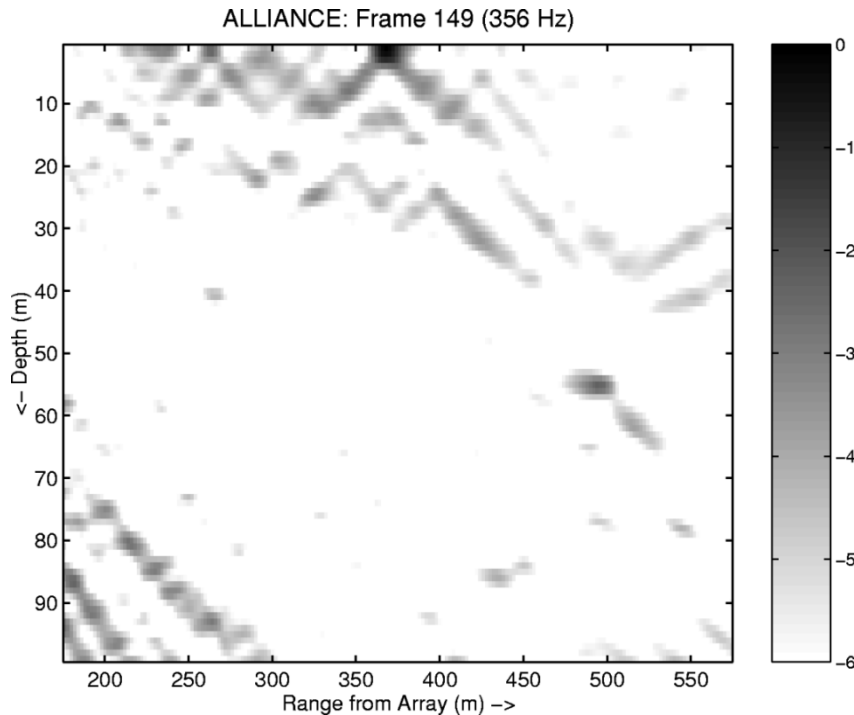


Fig. 14. Bartlett ambiguity surface of the ALLIANCE (dB) for frame 149 computed with optimized geometric and acoustic parameters.

Fig. 8 shows both the track of the tow ship, the NRV ALLIANCE, during the experiment and gives an indication of the local bathymetry in the test area. Over the entire track, the ship's depth sounder recorded a steady increase in depth from approximately 116 m to 124 m. Expendable bathy-thermograph casts showed an almost iso-velocity water column with a velocity of approximately 1520 m/s. The speed of the ALLIANCE was a steady four knots and the prevailing sea state was one.

In the area of the experiment, the sea floor has been fairly well characterized over the last 30 years [16]–[18] and is known to be flat and covered with a thin layer of clay and sand–clay sediments. For the purposes of the present study, this sediment layer was disregarded, as it has been noted in previous research that, at frequencies of a few hundred Hertz, its thickness is only a fraction of a wavelength [17]. Below the thin sediment layer is known to exist a reasonable approximation to an acoustic half-space with the approximate parameters $c_b \approx 1600$ m/s, $\rho_b \approx 1800$ kg/m³, and $\alpha_b \approx 0.15$ dB/λ [17]. In no results to date has there been evidence of significant shear wave propagation in the sea floor in this area and, hence, only compressional wave parameters were considered here. In any case, the assumption of a shear-wave velocity c_s within the plausible range for the bottom type in question ($c_s \ll c_w$) would lead mainly to an increased bottom loss [19], to which the current near-field inversion technique would be relatively insensitive.

To summarize, the acoustic model used here was a simple Pekeris environment with water–sound speed $c_w = 1520$ m/s, bottom density $\rho_b = 1800$ kg/m³, and bottom attenuation $\alpha_b = 0.15$ dB/λ. All other parameters were left to be determined by the GA search procedure.

A. A Commentary on the Experiment

The self-noise inversion dataset comprised 175 frames sampled at 30-s intervals. Only the first 10 s of each interval, or 60 000 samples at 6000 samples per second, were recorded. One novel aspect of this self-noise experiment was that two research vessels were involved. From about frame 60 to frame 107, the ALLIANCE, with its array towed approximately 330 m behind, was followed by the MANNING, at a range of approximately 900 m. The horizontal distance of the MANNING from the tail of the array was, therefore, approximately 300 m. The proximity of the two ships, while inviting the possibility of interference, turned out to be fortuitous in that inversions were possible, with each ship utilized alternately as a source of opportunity. Geoacoustic inversions could, therefore, be cross checked to improve confidence in their validity. At approximately frame 107, ALLIANCE started a 45° turn, while MANNING continued on track. Then, at around frame 122, MANNING left station and departed the area at increased speed without turning.

Fig. 9 is a plot of broad-band conventional beamformer output over the duration of the 175 frames of the experiment. The most striking aspect of this plot is the number and level of interfering contacts recorded. Of particular concern are the ships near the fore and aft endfire directions, which obscure the identification of multipath arrival structure from the ALLIANCE and MANNING along the lines of that simulated in Fig. 4.

B. Preprocessing

Figs. 10 and 11 show spectrograms computed from time-series beamformed in the fore and aft directions for the

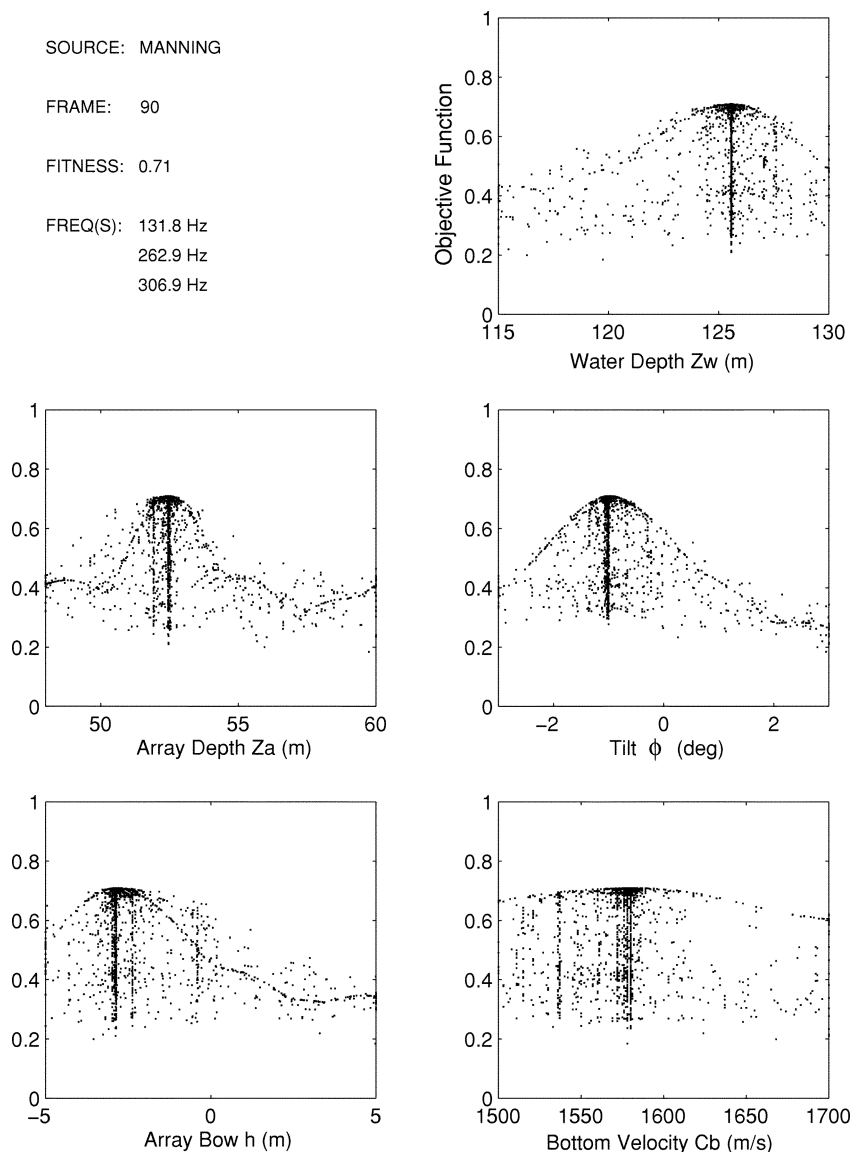


Fig. 15. Scatter plots of GA search for frame 90 (MANNING source).

duration of the experiment. From each 60 000-point frame, 14 Kaiser-Bessel windowed, 4096-point snap shots were averaged to estimate both the power-spectral densities (PSDs) and cross-spectral density matrices (CSDMs).

Elementary frequency tracking was used to follow small variations in tonal frequencies emitted by the source ships. The β parameter of 1.5π , used for the Kaiser-Bessel windows, resulted in a 3-dB analysis bandwidth of approximately 2.6 Hz. Given the level of interference from shipping traffic, it was found useful to incorporate additional spatial filtering of the snap-shot data. Preprocessing, therefore, entailed temporal windowing and 2-D FFT transformation of each snap shot, frequency masking to exclude certain ranges of spatial frequencies, and then inverse 2-D FFT transformation. With reference to Fig. 4, this spatial frequency cutoff was set to include arrival angles within 50° of endfire to capture most of the expected multipath arrivals from the ALLIANCE and MANNING. To retain the normalization of (11), identical filtering was applied to the replica vectors.

C. The Alliance

The NRV ALLIANCE is widely regarded as one of the quietest research vessels in the world. For this experiment, the ship was operating one level down from its all-electric ultra-quiet state with motive power supplied by an acoustically isolated gas-turbine system. This, along with the extreme level of interference, partly explains the lack of visible multipath structure from the ALLIANCE in Fig. 9. From Fig. 10, it is not immediately obvious which frequencies are associated with the ALLIANCE. Much of the harmonic structure in the spectrogram beamformed at 83° is related to an interfering ship, which can be seen in Fig. 9, to veer from within 20° of broadside in frame 1 to almost 80° in frame 90. In this study, the only discernible features of the tow-ship spectrum that gave convincing MFP peaks were the two closely spaced lines at 356 and 361 Hz, which can be seen to persist throughout the data.

Figs. 12 and 13 are scatter plots illustrating the parameters sampled during GA inversions using the ALLIANCE as a source in frames 149 and 160, respectively. Following each forward-

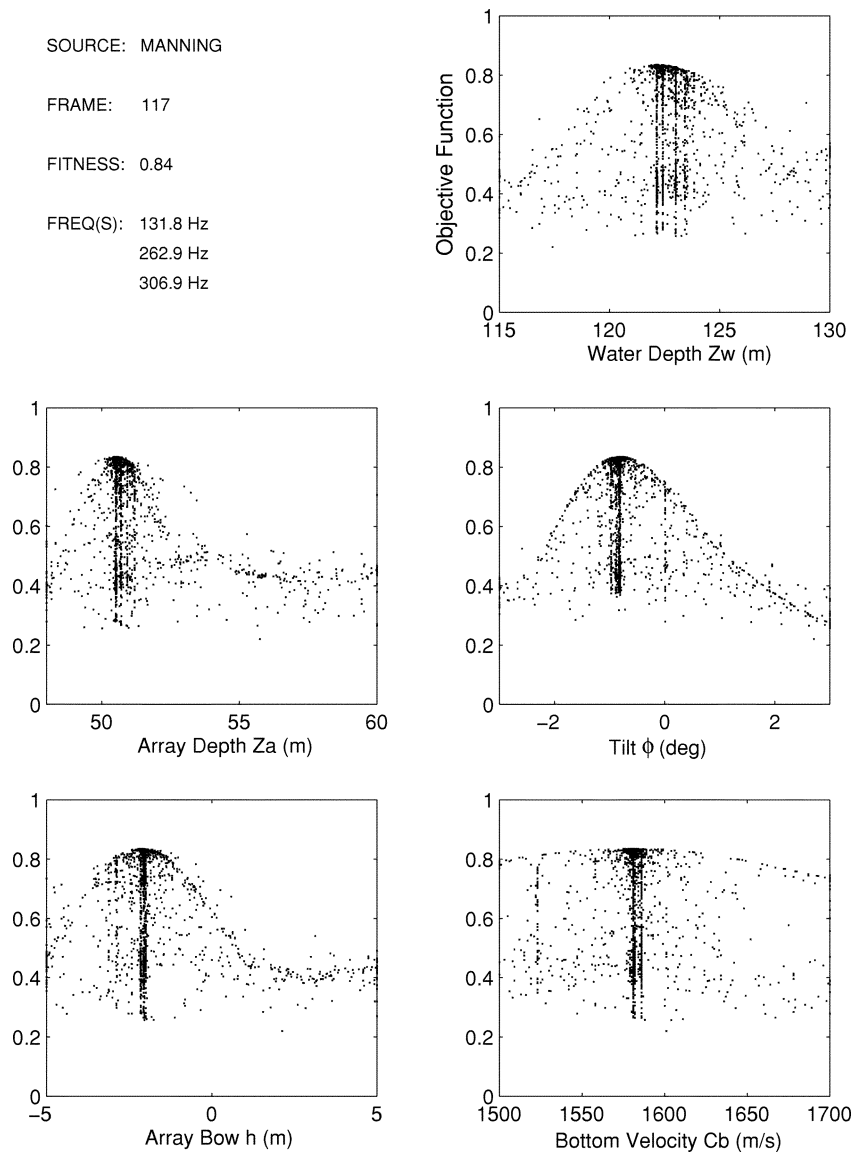


Fig. 16. Scatter plots of GA search for frame 117 (MANNING source).

model calculation, the objective function achieved was plotted with respect to each searched parameter. To reduce the dimensionality of the searches and to improve the stability of the results, it was found useful to process a few frames of data and later lock the source depth at the average value obtained. For the ALLIANCE, this effective source depth was found to be approximately 2 m. Similarly, the values of bottom density and attenuation were not optimized, but rather estimated from the literature. In any case, these two parameters only weakly influence the objective function in the near field, as discussed in Section II. With the ALLIANCE as a source, only the frames beyond 140 were found to give identifiable peaks in the c_b search range, probably because the signal-to-noise ratio (SNR) was higher there, as visible in Fig. 10. For inversion, the single line at 356 Hz was used. With a population size of 64 and other GA parameters at their default values, the total number of forward-model evaluations required for each inversion was approximately 4000.

Peaks in the c_b search range occurred at approximately 1580 m/s in both frames, which concurs reasonably well with values obtained by Jensen [16] (1600 m/s) and Gingras and Gerstoft [17] (1575 m/s). Relative to their maximum of unity, however, the fitness values below 0.2 achieved were marginal for inversion purposes, no doubt due to the combination of weak source level, strong interference, and lack of signature bandwidth.

In Fig. 12, it is clear that most of the geometric parameters have been reasonably well localized, especially the array tilt ϕ , which was seen earlier in Fig. 5 to have a strong sensitivity. Scatter plots of the objective function with respect to the water and array depths z_w and z_a , however, do have ambiguities manifesting as side lobes to the main sample clouds, which seem to have worsened in Fig. 13. Interestingly, these ambiguities do not appear to have affected the second c_b estimate, indicating robustness in the approach. Generally, it was observed here that under conditions of low SNR, scatter plots of the objective func-

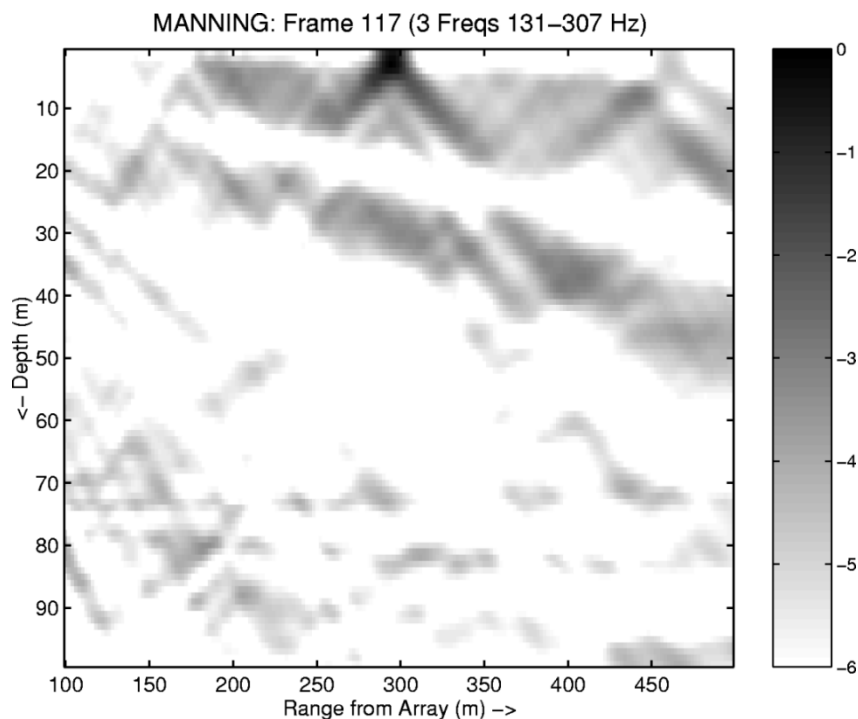


Fig. 17. Bartlett ambiguity surface of the MANNING (dB) for frame 117 computed with optimized geometric and acoustic parameters.

tion with respect to z_w and z_a first showed signs of the kind of break-up described. This behavior, in conjunction with the low fit values, indicates that the prevailing SNR may have been at the limit of what was useful for inversion.

Fig. 14 is the full MFP ambiguity surface calculated for the ALLIANCE using the optimized parameters from Fig. 12. Interestingly, the Alliance is a 93-m-long vessel, which would place the observed peak roughly amidships in line with the engine room. Modifying (11) to

$$B(\hat{\mathbf{m}}) = \frac{1}{K} \sum_{i=1}^K \left[\frac{\mathbf{w}_i^\dagger(\hat{\mathbf{m}}) \hat{\mathbf{R}}_i \mathbf{w}_i(\hat{\mathbf{m}})}{\|\mathbf{w}_i(\hat{\mathbf{m}})\|^4} \right] \quad (12)$$

with the replica vector $\mathbf{w}_i(\hat{\mathbf{m}})$ calculated specifically for the optimized parameters of Fig. 12 and the peak position in Fig. 14, the tonal source level of the ALLIANCE at 356 Hz was estimated to be 116 dB re $1 \mu\text{Pa}$. With reference to Fig. 10, it can be noted that the equivalent plane-wave signal level at the array of approximately 60 dB re $1 \mu\text{Pa}$ would correspond closely to that expected from the ALLIANCE if purely spherical spreading were assumed.

D. The Manning

In comparison with the ALLIANCE, the MANNING supplied a far-stronger source level and, as evident from Fig. 11, the harmonic features in its signature were quite pronounced after plane-wave beamforming. Between frames 90 and 117, the MANNING followed the ALLIANCE at a constant speed of 4 knots, having caught up from some distance behind to participate in the experiment. These frames were processed, using tonal frequencies of 131.8, 262.9, and 306.9 Hz, which were identified as stable and prominent peaks in the spectrogram.

With the same signal processing and GA parameters as before, 28 consecutive inversions were made, with Figs. 15 and 16 summarizing the first and last. Whereas the results obtained with the ALLIANCE suggested that the SNR was marginal for that case, the fitness obtained with the MANNING using three frequencies peaked at 0.84—high by inversion standards. Also, the projections of the sampling densities onto individual parameters show cleanly defined boundaries more analogous to the theoretical sensitivity curves in Fig. 5. In comparison with the calculated c_b sensitivity of approximately 7% for the theoretical case (source-array range = 400 m), the sensitivities seen in Figs. 15 and 16 appear slightly less, due to the range of the array being only 300 m. The locations of the peaks within the velocity search range occur at approximately 1580 m/s, concurring with the values obtained using the ALLIANCE. Fig. 17 illustrates the full ambiguity surface obtained for the MANNING when the optimized parameters of frame 117 were used. Estimation of the equivalent source level of the MANNING as per the ALLIANCE at the frequency of 306.9 Hz gave a value of 140 dB re $1 \mu\text{Pa}$.

Fig. 18 is the final figure presented here, which indicates that although the geometric sensitivity was low, due to the inadequate range of the array, reasonably consistent estimates of the bottom velocity were possible due to the relatively high source level presented by the MANNING.

VIII. CONCLUSION

This paper set out to evaluate the sensitivity of MFP as a solution to geoacoustic-inversion problems involving towed arrays. The importance of towing the array at a sufficient distance to allow eigenrays with grazing angles less than the critical angle

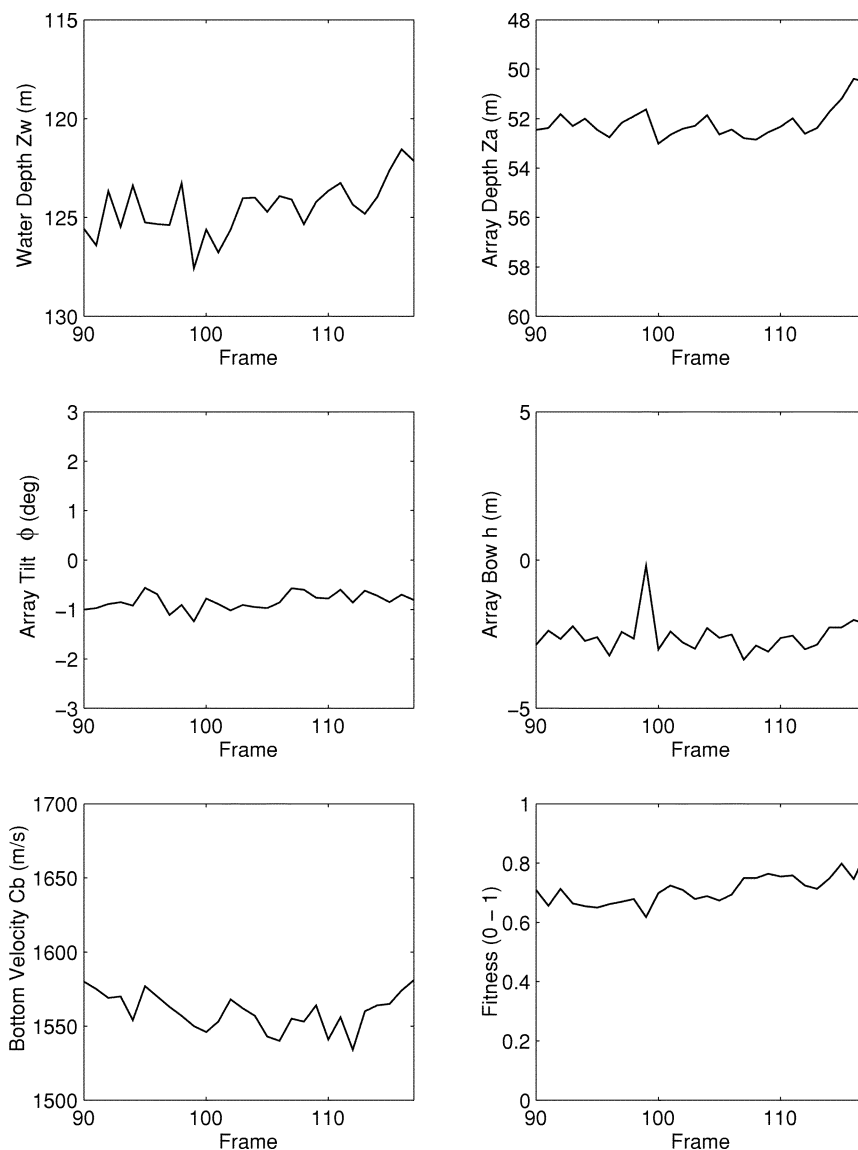


Fig. 18. GA inversion results versus frame (MANNING source).

was demonstrated both theoretically and experimentally. The theoretical study showed that near-field MFP is sensitive enough to facilitate robust first-order geoacoustic inversion; however, further work is needed to identify the limits of near-field sensitivity to more-complex environments.

Analysis of the experimental data confirmed the importance of global search algorithms for acoustic inverse problems, even in a case where it might be expected that the small multiplicity of paths between the source and receiver could make local searches tractable. GAs were effective and robust in spanning the search space of geometric and acoustic parameters, even under conditions of poor SNR and considerable array distortion.

Of the two ships used as sources of opportunity, neither was located sufficiently far from the array to yield optimal geoacoustic sensitivity; however, the experiment showed that there was still sufficient residual sensitivity to enable successful inversions. Equally, it was demonstrated that even very-quiet vessels, not much above the acoustic background of the open ocean,

potentially provide sufficient noise power to enable geoacoustic inversion. In this regard, it is believed that the source level provided by the ALLIANCE in this experiment was probably close to the minimum usable signal under the prevailing conditions.

REFERENCES

- [1] W. A. Kuperman, M. F. Werby, K. E. Gilbert, and G. J. Tango, "Beam forming on bottom-interacting tow-ship noise," *IEEE J. Ocean. Eng.*, vol. OE-10, pp. 290–298, July 1985.
- [2] A. Caiti, S. M. Jesus, and A. Kristensen, "Geoacoustic seafloor exploration with a towed array in a shallow water area of the strait of sicily," *IEEE J. Ocean. Eng.*, vol. 21, pp. 355–366, Oct. 1996.
- [3] S. M. Jesus and A. Caiti, "Estimating geoacoustic bottom properties from towed array data," *J. Comp. Acoust.*, vol. 4, no. 3, pp. 273–290, 1996.
- [4] M. Siderius, P. Nielsen, and P. Gerstoft, "Range-dependent seabed characterization by inversion of acoustic data from a towed receiver array," *J. Acoust. Soc. Amer.*, vol. 112, no. 4, pp. 1523–1535, 2002.
- [5] N. R. Chapman, R. M. Dizaji, and R. L. Kirilin, "Geoacoustic inversion using broad band ship noise," in *Proc. European Conf. on Underwater Acoustics (ECUA) '00*, 2000, pp. 787–792.

- [6] O. Gasparini, C. Camporeale, and A. Crise, "Introducing passive matched field acoustic tomography," *Il Nuovo Cimento*, vol. 20 C, no. 4, pp. 497–519, 1997.
- [7] R. J. Urick, *Principles of Underwater Sound*, 3rd ed. New York: McGraw Hill, 1983.
- [8] F. B. Jensen, W. A. Kuperman, M. B. Porter, and H. Schmidt, *Computational Ocean Acoustics*. New York: AIP, 1994.
- [9] H. Schmidt and F. B. Jensen, "A full wave solution for propagation in multilayered viscoelastic layered media with application to Gaussian beam reflection at fluid-solid interfaces," *J. Acoust. Soc. Amer.*, vol. 77, pp. 813–825, 1985.
- [10] W. T. Thomson, "Transmission of elastic waves through a stratified solid," *J. Appl. Phys.*, vol. 21, pp. 89–93, 1950.
- [11] N. A. Haskell, "The dispersion of surface waves in multilayered media," *Bull. Seism. Soc. Amer.*, vol. 43, pp. 17–34, 1953.
- [12] P. Gerstoft, "Inversion of seismoacoustic data using genetic algorithms and a posteriori probability distributions," *J. Acoust. Soc. Amer.*, vol. 95, no. 2, pp. 770–782, Feb. 1994.
- [13] —, "SAGA Users Guide 2.0, an Inversion Software Package," SACLANT Undersea Research Centre, SM-333, 1997.
- [14] P. Gerstoft and C. F. Mecklenbräuker, "Ocean acoustic inversion with estimation of a posteriori probability distributions," *J. Acoust. Soc. Amer.*, vol. 104, no. 2, pp. 808–819, 1998.
- [15] S. E. Dosso, "Quantifying uncertainty in geoacoustic inversion. I. A fast Gibbs sampler approach," *J. Acoust. Soc. Amer.*, vol. 111, no. 1, pp. 129–142, 2002.
- [16] F. B. Jensen, "Comparison of transmission loss data for different shallow water areas with theoretical results provided by a three-fluid normal-mode propagation model," in *Sound Propagation in Shallow Water*, O. F. Hastrup and O. V. Olesen, Eds. La Spezia, Italy: SACLANT ASW Research Centre, 1974, vol. CP-14, pp. 79–92.
- [17] D. F. Gingras and P. Gerstoft, "Inversion for geometric and geoacoustic parameters in shallow water: Experimental results," *J. Acoust. Soc. Amer.*, vol. 97, pp. 3589–3598, 1995.
- [18] D. D. Ellis and P. Gerstoft, "Using inversion techniques to extract bottom scattering strengths and sound speeds from shallow-water reverberation data," in *Proc. European Conf. on Underwater Acoustics (ECUA) '96*, 1996, pp. 557–562.
- [19] D. D. Ellis and D. M. F. Chapman, "A simple shallow water propagation model including shear wave effects," *J. Acoust. Soc. Amer.*, vol. 78, pp. 2087–2095, 1985.



David J. Battle (S'86–M'87) was born in Brisbane, Australia. He received the B.Eng. degree in electrical engineering from Queensland University of Technology, Brisbane, Australia, in 1988 and the Ph.D. degree in electrical engineering from the University of Sydney, Sydney, Australia, in 1999.

From 1991 to 2000, he conducted research in the fields of acoustic imaging and inverse scattering at the Lucas Heights Research Laboratories, Sydney, Australia. From 2001 to 2003, he was a Post-Doctoral Fellow in the Marine Physical Laboratory,

Scripps Institution of Oceanography, University of California, San Diego. Since 2003, he has been a Research Engineer in the Ocean Engineering Department, Massachusetts Institute of Technology, Cambridge, MA. His research interests include ocean acoustic inverse problems and signal processing, particularly in connection with novel applications of autonomous underwater vehicles.



Peter Gerstoft (M'03) received the M.Sc. and Ph.D. degrees from the Technical University of Denmark, Lyngby, in 1983 and 1986, respectively, and the M.Sc. degree from the University of Western Ontario, London, ON, Canada, in 1984.

From 1987 to 1992, he was employed at Ødegaard and Dannekiold-Samsøe, Copenhagen, Denmark, working on forward modeling and inversion for seismic exploration, with a year as Visiting Scientist at the Massachusetts Institute of Technology, Cambridge. From 1992 to 1997 he was Senior Scientist at SACLANT Undersea Research Centre, La Spezia, Italy, where he developed the SAGA inversion code, which is used for ocean acoustic and electromagnetic signals. Since 1997, he has been with the Marine Physical Laboratory, University of California, San Diego. His research interests include global optimization; modeling; and inversion of acoustic, elastic, and electromagnetic signals.



William A. Kuperman has conducted theoretical and experimental research in ocean acoustics and signal processing at the Naval Research Laboratory, SACLANT Undersea Research Centre, La Spezia, Italy, and at the Scripps Institution of Oceanography (SIO), University of California, San Diego.

He currently is a Professor at SIO and the Director of its Marine Physical Laboratory.



William S. Hodgkiss (S'68–M'75) was born in Bellefonte, PA, on August 20, 1950. He received the B.S.E.E. degree from Bucknell University, Lewisburg, PA, in 1972 and the MS and Ph.D. degrees in electrical engineering from Duke University, Durham, NC, in 1973 and 1975, respectively.

From 1975 to 1977, he was with the Naval Ocean Systems Center, San Diego, CA. From 1977 to 1978, he was a Faculty Member in the Electrical Engineering Department, Bucknell University, Lewisburg, PA. Since 1978, he has been a Member of the Faculty, Scripps Institution of Oceanography, University of California, San Diego, and on the staff of the Marine Physical Laboratory, where he is currently Deputy Director. His present research interests are in the areas of adaptive array processing, propagation modeling, and environmental inversions with applications of these to underwater acoustics and electromagnetic wave propagation.

Dr. Hodgkiss is a Fellow of the Acoustical Society of America.



Martin Siderius received the B.S. degree in physics from Western Washington University, Bellingham, in 1986. He received the M.S.E.E. and Ph.D. degrees, both in electrical engineering, from the University of Washington, Seattle, in 1992 and 1996, respectively.

He was an Engineer with Baird Corporation, Bedford, MA, from 1986 to 1987 and with Bio-Rad, Cambridge, MA, from 1987 to 1990. From 1990 to 1996, he was a Research Assistant at the Applied Physics Laboratory at the University of Washington.

From 1996 to 2001, he was on the scientific staff in the Acoustics Department at the NATO SACLANT Undersea Research Centre, La Spezia, Italy. He joined Science Applications International Corporation in July 2001 and is currently a Senior Scientist in the Ocean Sciences Division. His research interests include underwater acoustics and signal processing.